The localization and crystallographic dependence of Si suboxide species at the SiO_2/Si interface

P. J. Grunthaner, M. H. Hecht, and F. J. Grunthaner
Jet Propulsion Laboratory, California Institute of Technology, Pasadena, California 91109

N. M. Johnson
Xerox Palo Alto Research Center, Palo Alto, California 94304

(Received 17 February 1986; accepted for publication 12 September 1986)

X-ray photoemission spectroscopy has been used to examine the localization and crystallographic dependence of Si^{+1}, Si^{+2}, and Si^{+3} suboxide states at the SiO_2/Si interface for (100)- and (111)-oriented substrates with gate oxide quality thermal oxides. The Si^{+1} and Si^{+2} states are localized within 6–10 Å of the interface while the Si^{+3} state extends ~30 Å into the bulk SiO_2. The distribution of Si^{+1} and Si^{+2} states shows a strong crystallographic dependence with Si^{+2} dominating on (100) substrates and Si^{+1} dominating on (111) substrates. This crystallographic dependence is anticipated from consideration of ideal unreconstructed (100) and (111) Si surfaces, suggesting that (1) the Si^{+1} and Si^{+2} states are localized immediately within the first monolayer at the interface and (2) the first few monolayers of substrate Si atoms are not significantly displaced from the bulk. The total number of suboxide states observed at the SiO_2/Si interface corresponds to 94% and 83% of a monolayer for these (100) and (111) substrates, respectively. We speculate that the remaining interfacial substrate Si atoms that are not associated with bonding to oxygen are bonded to impurity species.

I. INTRODUCTION

Probing the morphology and chemical structure of the SiO_2/Si interface is a problem that has been addressed over the last 10–15 years using a variety of spectroscopic techniques. Interest has been sustained by the realization that interfacial properties play a critical role in establishing overall metal-oxide-semiconductor (MOS) device performance. Numerous techniques have been used to examine the SiO_2/Si system, including cross-sectional transmission microscopy,[1] ion scattering,[2–4] Auger spectroscopy,[5,6] photoelectron spectroscopy,[7–10] and spectroscopic ellipsometry.[11] An examination of the literature shows that most structural determinations of the interfacial width in the SiO_2/Si system reflect the minimum resolvable limits of the probe employed and are consistent with a SiO_x transition region approximately one monolayer in thickness. However, the details of the local atomic chemistry within this SiO_x transition region remain largely unknown, primarily because of the experimental difficulty involved in examining a single monolayer buried beneath an oxide overlayer.

Core-level photoemission is particularly well suited for examining the SiO_x transition region because of its sensitivity to the local chemical environment around a given atom. In early studies by Grunthaner *et al.*[8] numerical enhancement techniques were used on Si 2*p* core level spectra of SiO_2 on Si(100) to establish the presence of Si in three intermediate oxidation states, attributable to Si^{+1}, Si^{+2}, and Si^{+3}. Estimates of the relative suboxides intensities were made using less quantitative methods than in the current work. Spectral difference methods were also used to look for the presence of Si^{+1} and Si^{+3} species.[12] Hollinger and Himpsel were later able to directly observe the presence of these Si suboxide states at the SiO_2/Si interface using synchrotron radiation to examine the Si 2*p* core level.[9] They reported that the distribution of these suboxide states was essentially independent of the substrate crystallographic orientation and SiO_2 thickness. Hattori and Suzuki also examined with photoemission the crystallographic dependence of the suboxide distribution on (100), (111), and (110) substrates.[10] They concluded that the Si^{+3} suboxide state was not localized at the immediate SiO_x transition layer, but was instead distributed throughout the bulk of the SiO_2 overlayer.

In this paper, we use x-ray photoemission spectroscopy (XPS) to address the critical question of the localization of the intermediate oxides of silicon and examine the detailed composition of the SiO_x transition layer for thermal SiO_2 on (100)- and (111)-oriented Si. In contrast to Hollinger and Himpsel,[9] we observe a strong dependence of the suboxide distribution upon crystallographic orientation. We discuss the possible sources of discrepancy between our data and those of others and, furthermore, suggest that the suboxide distribution can be used to characterize the distribution of structural imperfections and impurities at the interface.

There are five possible formal oxidation states for silicon as illustrated in Fig. 1. Elemental Si and SiO_2 are denoted as Si^0 and Si^{+4} states, respectively. The suboxide states are characterized by bonding to 1, 2, or 3 oxygen atoms and are denoted as Si^{+1}, Si^{+2}, and Si^{+3} states, respectively. The Si 2*p* XPS spectrum of a thin oxide on silicon is characterized by two major features separated by approximately 4 eV binding energy as illustrated in Fig. 2(a). The energy scale is referenced to the substrate peak position, which falls at 99.6 eV for this particular sample. The substrate line can be observed through the oxide overlayer because of the relatively long electron mean free path (37 ± 4 Å for Si 2*p* electrons traversing thick SiO_2 overlayers[13]). The broad peak 4 eV above the substrate signal corresponds to photoelectrons emitted from SiO_2. If the intensity axis in Fig. 2(a) is expanded as shown in Fig. 2(b), the Si suboxide signals can be observed in the region between the substrate and SiO_2 peaks.

 0021-8979/87/020629-10$02.40

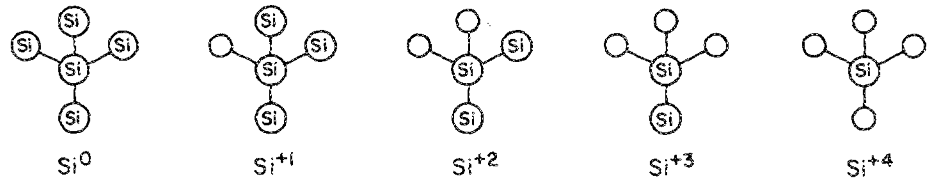

FIG. 1. Illustration of the five possible formal oxidation states for silicon. The small circles represent oxygen atoms.

For clarity, the Si 2*p* line shapes for bulk SiO_2 and elemental Si have been overplotted with the data to emphasize the difference between these bulk constituents and the original spectrum. The peak positions of the Si^{+1}, Si^{+2}, and Si^{+3} species, indicated with arrows, agree with values previously reported.[8,9] Relative to the Si substrate, the suboxide species are observed at 1.0, 1.7, and 2.6 eV, respectively. Quantitative information on the relative intensities of these species has been obtained by fitting the component peaks using a nonlinear least-squares procedure as described in Sec. III.

II. EXPERIMENT

Data presented in this paper pertain to samples prepared using (100)- and (111)-oriented Czochralski-grown, *p*-type (boron) silicon wafers with resistivities of 20–30 Ω cm and > 100 Ω cm, respectively. Specimens were prepared at Xerox Palo Alto Research Center by first precleaning with an electronic-grade detergent (Aquenet), followed by 10 min in boiling $NH_4OH:H_2O_2:H_2O$ (1:1:5) and a deionized (DI) water rinse. Samples were then cleaned using the following procedure: DI rinse, $HF:H_2O$ (1:50) dip, DI rinse, 10 min in boiling $H_2SO_4:H_2O_2$ (1:1), DI rinse, $HF:H_2O$ (1:50) dip, DI rinse, N_2 blow dry. Specimens were oxidized at 900 °C in dry O_2 for approximately 3 min and fast pulled under O_2. The resulting oxide thicknesses were estimated to be 40–50 Å by ellipsometric measurement. Similar results were found on six Si(100) samples and two Si(111) samples, reflecting a variety of processing conditions.

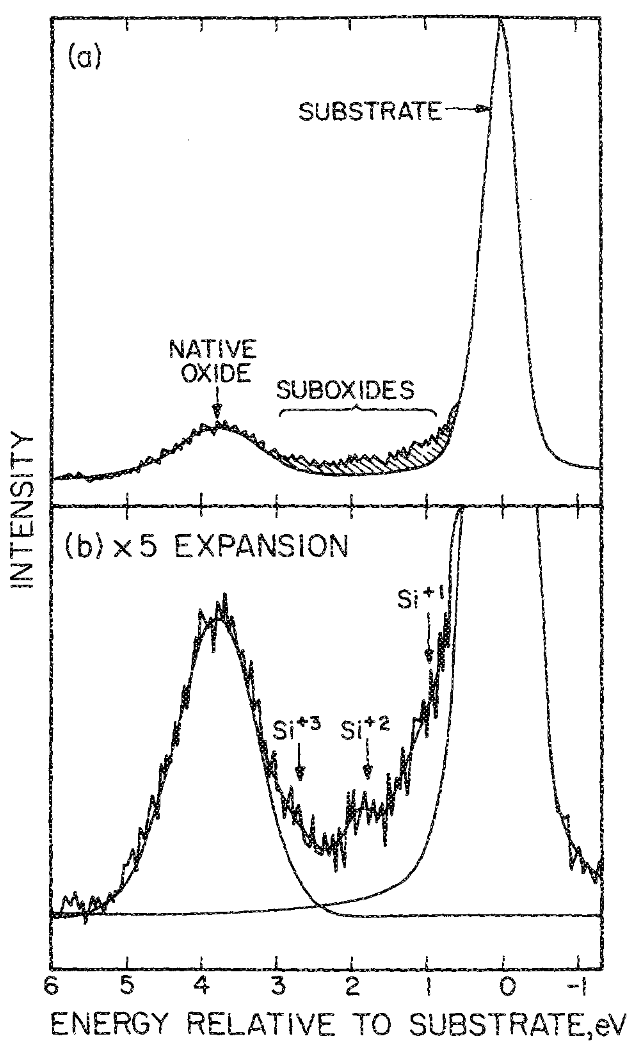

FIG. 2. (a) Typical Si 2*p* XPS spectrum of a thin native oxide on silicon. The spin-orbit doublet has been removed. (b) An expansion of the intensity axis of the spectrum shown in (a).

Si 2*p* spectra were obtained as a function of oxide thickness by chemically thinning the oxide using a spin-etch procedure performed in a N_2 flushed dry box connected to the sample introduction chamber of the spectrometer. The N_2 is provided by liquid-N_2 evaporation. The spin-etch procedure involves spinning the specimen at 3600 rpm while adding dropwise a solution of 10% electronic-grade HF in United States Pharmacopeia (USP) grade absolute ethanol.[14] The samples were rinsed with ethanol using the same technique. In a previous study,[15] which compared photoemission results on samples profiled by this spin-etch procedure with samples "profiled" by varying the incident photon energy, we demonstrated that the spin-etch removal of the oxide does not perturb the oxide structure.

III. DATA REDUCTION

Figure 3 illustrates the procedure used to obtain quantitative information on the Si suboxide intensities. This procedure is the same as that used by Hollinger and Himpsel.[9] A typical Si 2*p* spectrum of a thin thermal oxide on Si is shown in Fig. 3(a). The solid line in Fig. 3(b) displays the same data, but without the intrinsic spin-orbit doublet. The spin-orbit doublet has been removed by dividing the Fourier transform of the data by the Fourier transform of two δ functions with an energy separation and intensity ratio corresponding to the known spin-orbit-split components. The inverse transform of this quotient permits one to examine the data with each chemical species contributing a single peak to the spectrum rather than two spin-orbit-split components. The peak positions for the three suboxide species are indicated by dashed lines. The dotted line corresponds to the appropriate sum of bulk substrate and SiO_2 components. Quantifying the suboxide intensity requires removing the contributions from these intense bulk signals, the tails of which overlap the suboxide region. For this analysis, the individual components of the spectrum are modeled (estimated) by a fitting procedure based on least-squares minimization. The individual components were constrained as follows:

(1) The (111) substrate component was fitted using the

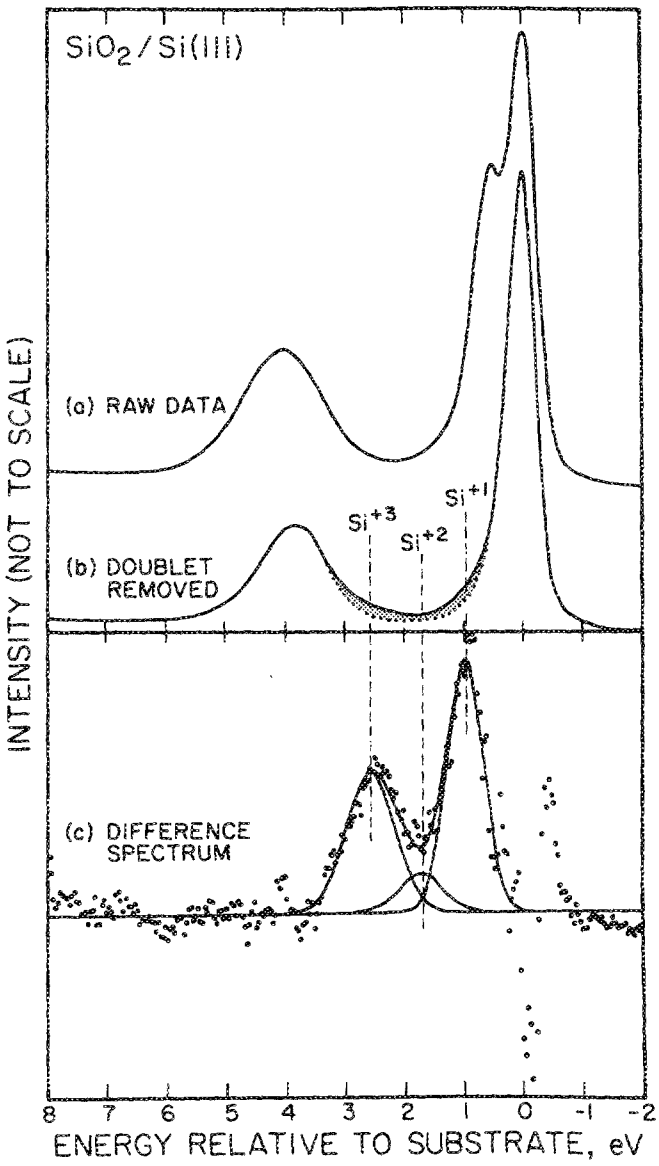

FIG. 3. (a) Si 2*p* XPS spectrum of a thin thermal oxide on Si(111). (b) Same data as in (a), but with the spin-orbit doublet removed. The dotted line is the sum of the bulk substrate and SiO_2 components. (c) Difference spectrum between the solid and dotted line in (b).

Si 2*p* spectrum from a clean Si(111) substrate. The Si 2*p* spectrum from clean Si(100) was used for the substrate component for data obtained on (100) substrates.

(2) The Si^{+1}, Si^{+2}, and Si^{+3} components were fitted with symmetric Gaussians with energy positions constrained to those previously observed for these suboxide species (1.0, 1.7, and 2.6 eV, respectively, relative to the Si substrate). The full width at half maximums (FWHM's) were allowed to vary within a small range of values normally observed for oxide species. The resulting FWHM values are discussed further below. The peak intensities were constrained to be positive. For very small peaks where statistical scatter dominates the fit, the result may be considered to be an upper limit for this reason.

(3) The SiO_2 component was fitted using the sum of two Voight line shapes, consistent with the observation that the near-interfacial SiO_2 region is structurally distinct from bulk SiO_2.[8,14–18] Because of this structural distinction near the SiO_2/Si interface, the SiO_2 envelope must be fitted with two components whose relative intensities vary as a function of SiO_2 thickness. Indeed, we observe that the SiO_2 manifold cannot be fitted with a single Gaussian or Voight lineshape. The energy positions for the bulk and near-interfacial SiO_2 components were constrained to agree with the energy positions observed for thick and thin (<50 Å) oxides (3.8 and 4.4 eV, respectively, relative to the substrate). The FWHM values were allowed to vary within a small range typical of oxide signals.

The dotted line in Fig. 3(b) represents the sum of the substrate and both SiO_2 components as determined from the least-squares procedure described above. The shaded region corresponds to that intensity which cannot be attributed to the elemental Si from the substrate or stoichiometric SiO_2. The difference between the solid and dotted lines in Fig. 3(b) is plotted in Fig. 3(c), along with the Si^{+1}, Si^{+2}, and Si^{+3} components determined from the least-squares procedure. The intensities of the suboxide signals are determined by integrating these components.

There is inherent error in a least-squares determination of peak components in which the detailed line shapes are not known. Symmetrical Gaussians were used to approximate the suboxide components in the procedure used here. The use of a different line shape would result in different integrated intensities, with the magnitude of the difference depending upon how much variation is permitted in the line shape. To examine this inherent error, we fitted the suboxide components with asymmetrical Gaussian as well as Voight line shapes with completely unconstrained asymmetry and full-width parameters. We observed the resulting integrated intensities to vary by 10–20%. Since the trends in suboxide distributions discussed below involve tenfold changes in suboxide intensities, this inherent error does not affect any conclusions of this paper.

The FWHM values obtained for the Gaussians fitted to the three suboxide states in Fig. 3(c) increase in the order Si^{+1} (0.7 eV) $<Si^{+2}$(0.9 eV) $<Si^{+3}$(1.0 eV). This trend was observed in all fits and is consistent with the notion that the width of the signal should increase as the number of Si–O bonds around a given Si atom increases. The Si substrate consists of an ordered lattice and, therefore, has the narrowest FWHM. At the other extreme, the SiO_2 network consists of long-range disorder, permitted by the flexibility of the Si–O–Si bond angle.[19] This long-range disorder results in a broadening of the SiO_2 signal relative to an ordered system such as α-quartz. The Si suboxide signals should broaden in the order $Si^{+1} < Si^{+2} < Si^{+3}$ as the increasing number of Si–O–Si bridging bonds increase the degrees of structural freedom.

We consistently observe for both (100)- and (111)-oriented substrates that the Si substrate signal obtained with an oxide overlayer cannot be precisely fit using the spectrum obtained from a oxide-free Si substrate. This results in the scatter in the points of the difference curve around 0 eV in Fig. 3(c). Part of the discrepancy is due to oxide-induced disorder of the Si substrate, as observed using ion channeling.[4,20] In addition, the clean Si sample used for comparison

has been prepared by a chemical stripping procedure which results in a hydrogen-terminated surface. The monolayer of Si–H bonds enhances the low binding energy side of the Si $2p$ peak.

IV. RESULTS AND DISCUSSION

A. Localization of suboxide species at the SiO_2/Si interface

In this section we provide evidence that the suboxide states are localized at the SiO_2/Si interface and do not extend into the bulk SiO_2. The spatial distribution of suboxide states within the SiO_2 overlayer can be straightforwardly examined by determining the ratio of the suboxide intensity to the substrate intensity as a function of SiO_2 thickness. If the suboxide states are localized immediately at the SiO_2/Si interface, the ratio of these signals will be independent of SiO_2 thickness since both the suboxide and substrate signals are equally attenuated by the SiO_2 overlayer. If, however, the suboxide species are dispersed within the SiO_2, the suboxide to substrate intensity ratio will be a strong function of SiO_2 thickness.

The Si $2p$ spectra obtained as a function of SiO_2 thickness for (100)-oriented Si are shown in Fig. 4(a). The spin-orbit doublet has been removed as discussed in Sec. III. A fourfold expansion of the intensity axis is shown in Fig. 4(b) to emphasize the suboxide region. The intensities of the Si substrate, SiO_2, and suboxide components have been determined using the fitting procedure discussed in Sec. III and, after normalization by the substrate intensity, are plotted in Fig. 5. The SiO_2 thickness on the x axis is expressed in units of the average electron mean free path. This reduced thickness is obtained from the following expression:

$$d/\langle\lambda_{\text{oxide}}\rangle = \sin\theta \ln(R_1/C + 1), \tag{1}$$

where d is the SiO_2 thickness,

$$R_1 = I_{\text{oxide}}(d)/I_{\text{Si}}(d),$$

$$C = (\rho_{\text{oxide}}\lambda_{\text{oxide}})/(\rho_{\text{Si}}\lambda_{\text{Si}}),$$

$I_{\text{oxide}}(d)$ and $I_{\text{Si}}(d)$ are the intensities of the SiO_2 and sub-

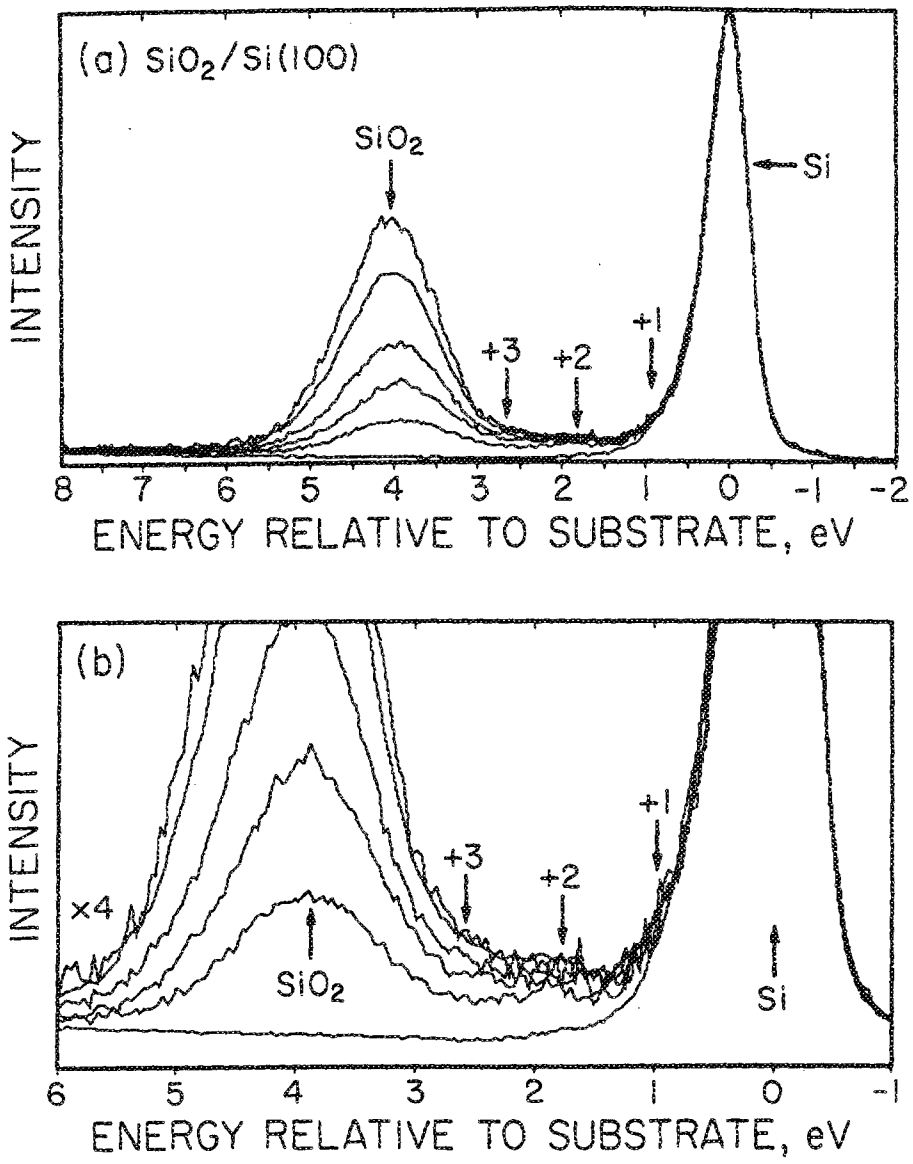

FIG. 4. (a) Si $2p$ XPS spectra obtained as a function of SiO_2 thickness for Si(100). The spin-orbit doublet has been removed. (b) Fourfold expansion of the intensity axis in (a) to emphasize the suboxide components.

strate Si signals with an oxide overlayer of thickness d, ρ_{oxide} and ρ_{Si} are atomic densities of Si in SiO_2 and elemental Si, λ_{oxide} and λ_{Si} are electron mean free paths for Si 2p photoelectrons in SiO_2 and elemental Si, and θ is the exit angle of photoelectrons (fixed for all experiments).

The SiO_2 thickness is expressed in this reduced form to emphasize that the x axis is not a *linear* measure of thickness since the electron mean free path, λ_{oxide}, is different in the near-interfacial SiO_2 region as compared to bulk SiO_2.[13,15,21] Although the thickness dependence of λ_{oxide} cannot be independently determined in these experiments, the ratio C can be experimentally determined.[21] We have observed C to vary from approximately 0.32 to 0.52 for thermal SiO_2 on Si, depending upon the conditions under which the oxide is grown.[21] The error bars in Fig. 5 represent this uncertainty in the value of C. As d decreases, the error due to C also decreases as a consequence of the logarithmic relationship. An alternative approach to calculating the reduced oxide thickness, $d/\langle\lambda_{oxide}\rangle$, involves the ratio of the substrate intensity with an oxide overlayer to the intensity of a clean Si substrate, $I_{Si}(d)/I_{Si}(0)$. However, the experimental intensities in this approach are subject to errors caused by a variety of factors affecting absolute signal intensity, such as a variation in x-ray flux and surface residues between etches. We have found that these errors exceed the errors generated by the lack of knowledge of C in Eq. (1).

Several observations can be made from Fig. 5. First, the Si^{+1} signal is at our detection limit, and is at least one order of magnitude weaker than that observed for the dominant Si^{+2} and Si^{+3} species. The normalized suboxide intensities for Si^{+2} and Si^{+3} show no dependence upon SiO_2 thickness until the oxide thickness is less than $\sim 0.35\langle\lambda_{oxide}\rangle$. Assuming a value of λ_{oxide} of 30 Å, as determined by XPS studies of thin SiO_2 layers on Si,[21,22] this corresponds to an oxide thickness of ~ 10 Å. Below ~ 10 Å in oxide thickness, the normalized intensities of the Si^{+2} and Si^{+3} species begin to decrease as these species are removed with the chemical etchant. From this one may conclude that these suboxide species are localized within 10 Å of the SiO_2/Si interface. This figure obviously includes the penetration range of the etchant as well as the true suboxide distribution. The abruptness of the knee in the curve, in fact, confirms the uniformity of the etch profile.

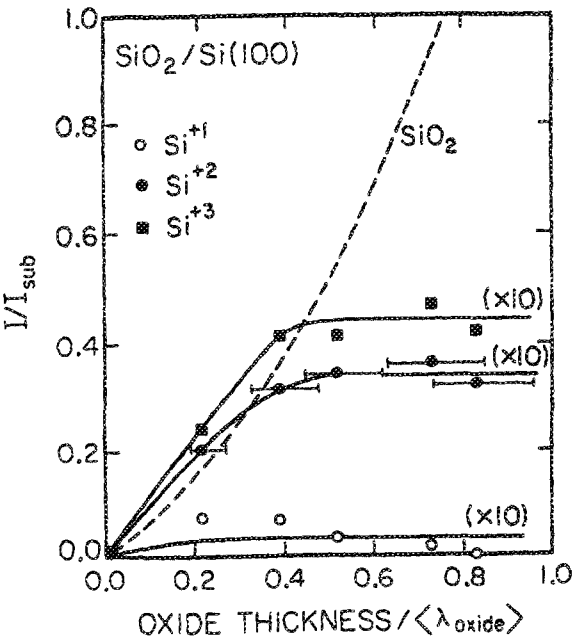

FIG. 5. Normalized intensities of the SiO_2 and suboxide components plotted as a function of SiO_2 thickness for SiO_2 on Si(100). The x axis is expressed in units of the electron mean free path.

For comparison, the Si 2p spectra obtained as a function of SiO_2 thickness for a (111)-orientated substrate are plotted in Fig. 6(a) with the spin-orbit doublet removed. To emphasize the suboxide region, a fourfold expansion of the intensity axis is plotted in Fig. 6(b). After fitting the substrate, SiO_2, and suboxide components in the spectra, one obtains the normalized intensity plot shown in Fig. 7. For the case of a (111) substrate, we observe the normalized Si^{+2} intensity to be considerably weaker than that found for the Si^{+1} and Si^{+3} species. The normalized Si^{+1} intensity is independent of SiO_2 thickness until the SiO_2 thickness is less than $\sim 0.2\langle\lambda_{oxide}\rangle$, which corresponds to ~ 6 Å. Below ~ 6 Å, the intensity of the Si^{+1} species decreases, from which one may conclude that this species is localized within ~ 6 Å of the SiO_2/Si(111) interface. The normalized Si^{+3} intensity shows a modest dependence upon SiO_2 thickness, falling off rapidly below $\sim 0.3\langle\lambda_{oxide}\rangle$. From this intensity behavior one may conclude that, in addition to a Si^{+3} component localized at the immediate SiO_2/Si(111) interface, a small amount of a Si^{+3} species must extend into the SiO_2. Because the normalized Si^{+3} intensity is not increasing exponentially, as does the normalized SiO_2 intensity, the Si^{+3} is not uniformly distributed within the SiO_2, but rather its concentration must be decreasing rapidly with increasing distance from the SiO_2/Si interface. The behavior of the Si^{+3} signal is discussed in more detail below.

We have examined the distribution of suboxide species for a variety of oxidation conditions[23] and, without exception, always observe the Si^{+1} and Si^{+2} signal intensities to be independent of SiO_2 thickness until within 6–10 Å of the interface.[24] The behavior of the Si^{+3} intensity is less consistent. In Fig. 5, we observe that the Si^{+3} suboxide is entirely localized within ~ 10 Å of the SiO_2/Si interface, but, in general, we have observed a modest dependence of the Si^{+3} intensity on SiO_2 thickness out to ~ 30 Å away from the interface,[23] as is the case shown in Fig. 7. We suggest that this behavior of the Si^{+3} intensity is due to the presence of two Si^{+3} species: (1) a Si^{+3} species localized immediately at the SiO_2/Si interface (a Si atom bonded to one substrate Si atom and three oxygen atoms, as diagrammed in Fig. 1) and (2) a Si^{+3} species due to hydrogen bonding in the SiO_2 network (a Si atom bonded to one hydrogen atom and three oxygen atoms within the SiO_2 network). The difference in binding energy between these two Si^{+3} species is expected to be only a few tenths of an eV and the least-squares fitting procedure used here could not discriminate between the species. It is also possible that the Si^{+3} signal observed within the first 30 Å of SiO_2 is due to nonstoichiometric oxide (the presence of Si–Si bonds). We are prejudiced, however, toward an explanation involving Si–H bonds since other techniques [in-

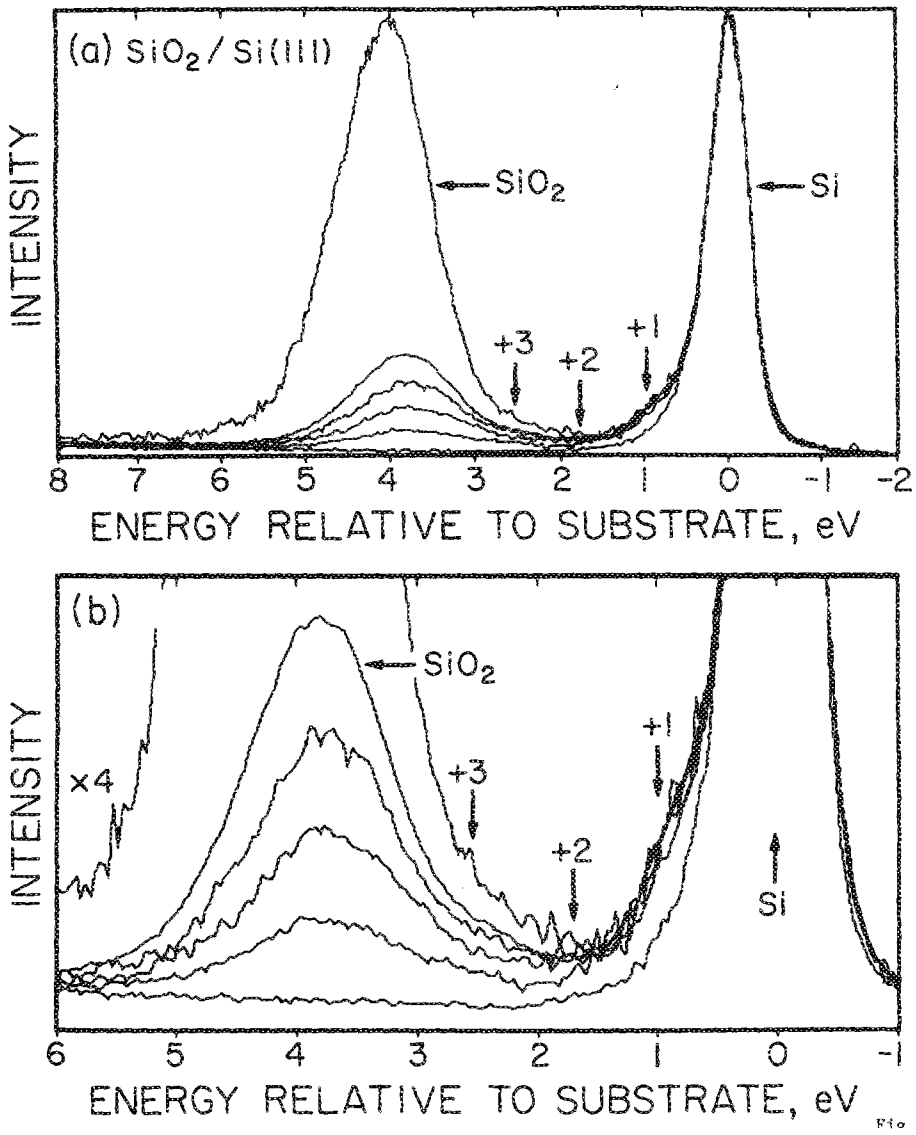

FIG. 6. (a) Si $2p$ XPS spectra obtained as a function of SiO_2 thickness for SiO_2 on Si(111). The spin-orbit doublet has been removed. (b) Fourfold expansion of the intensity axis in (a).

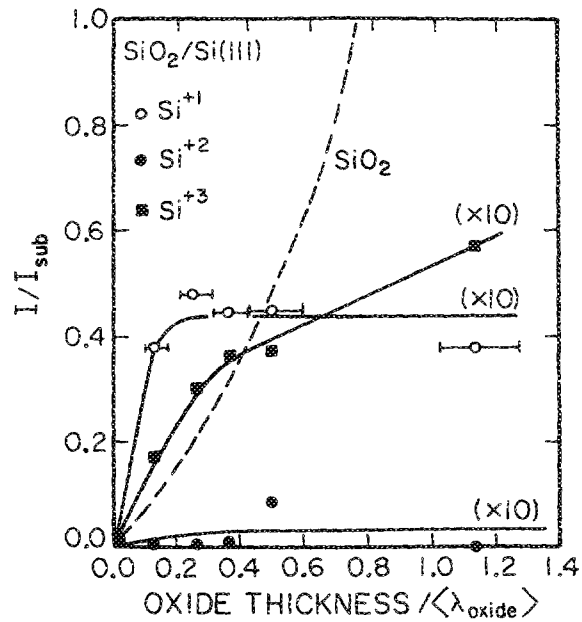

FIG. 7. Normalized intensities of the SiO_2 and suboxide components plotted as a function of SiO_2 thickness for SiO_2 on Si(111). The x axis is expressed in units of the electron mean free path.

frared spectroscopy[25] and secondary-ion mass spectroscopy[26] (SIMS)] have identified significant hydrogen concentrations in the interfacial region. Furthermore, the concentration of Si^{+3} states we observe extending into the near-interfacial SiO_2 is of the same order of magnitude as the hydrogen concentration observed by ir and SIMS.

The number of suboxide states corresponding to the observed intensity ratios can be calculated using the following expression:

$$N = \rho_{Si}\lambda_{Si}R_2 \sin\theta p/(e^p - 1), \tag{2}$$

where N is the mean surface density of suboxide states in cm^{-2}, R_2 is the suboxide to substrate intensity ratio, $p = d/(\langle\lambda_{oxide}\rangle \sin\theta)$, and ρ_{Si}, λ_{Si}, θ, d, and λ_{oxide} are as defined for Eq. (1). For small values of p,

$$p/(e^p - 1) \to 1. \tag{3}$$

Thus, the calculation of N is not affected by the imprecise knowledge of $\langle\lambda_{oxide}\rangle$. The values of R_2 used to calculate N were determined by averaging the normalized suboxide intensities in Figs. 5 and 7 over the region in which the intensities are constant. The exception to this is the Si^{+3} intensity ratio for SiO_2 on Si(111) in Fig. 7. For this case, we used the

normalized Si^{+3} ratio corresponding to an oxide thickness of $0.3\langle\lambda_{oxide}\rangle$. Here we are making the assumption that all Si^{+3} species below $0.3\langle\lambda_{oxide}\rangle$ are species at the immediate SiO_2/Si interface, while above $0.3\langle\lambda_{oxide}\rangle$ the intensity ratio contains contributions from Si^{+3} species dispersed in the near-interfacial SiO_2 network. The values for ρ_{Si} and λ_{Si} were taken as 5.00×10^{22} atoms/cm^2 and 26 Å, respectively (the escape depth in the substrate is significantly less than in the oxide). The calculations of suboxide areal densities for SiO_2 on Si(100) and Si(111) are summarized in Table I and plotted as a histogram in Fig. 8.

The total number of Si^{+1}, Si^{+2}, and Si^{+3} suboxide states observed at the SiO_2/Si(100) interface corresponds to 6.4×10^{14} states/cm^2. Assuming an areal density of substrate Si atoms for the (100) surface of 6.8×10^{14} atoms/cm^2, [27] this corresponds to ~94% of a monolayer of suboxide species at the SiO_2/Si(100) inteface. For the (111)-oriented substrate, 6.5×10^{14} suboxide states/cm^2 are found, excluding those Si^{+3} species extending beyond $0.3\langle\lambda_{oxide}\rangle$. Assuming an areal density of 7.8×10^{14} atoms/cm^2 for the Si(111) surface,[27] this corresponds to ~83% of a monolayer of suboxides at the SiO_2/Si(111) interface. This is in good agreement with previous studies in which we examined the suboxide distribution at the SiO_2/Si(100) interface following a variety of oxidation conditions.[23] The suboxide concentrations from the previous study are also summarized in Table I for comparison. Without exception, we always observe that less than a full monolayer of interfacial substrate Si atoms exist as suboxide species.

We postulate that the remaining fraction of a monolayer of interfacial substrate Si atoms that are not associated with bonding to oxygen are in a configuration which does not contribute to the suboxide intensity. In particular, the termination of substrate Si atoms by hydrogen can readily account for the remaining interfacial bonds since no direct measure of H-bonded species can be easily resolved by XPS (the H-terminated species are not resolvable from the bulk substrate signal). We do observe core-level signals corresponding to low levels of carbon and fluorine, most of which is present as contamination on the oxide surface rather than as interfacial contamination. However, these impurities, if bonded to Si at the interface, will produce a significant chemical shift of the Si 2*p* level in the same direction as that produced by oxygen bonds. As a result, a Si atom bonded to these impurities will be "miscounted" as a suboxide state and therefore cannot account for the "missing" interfacial Si atoms.

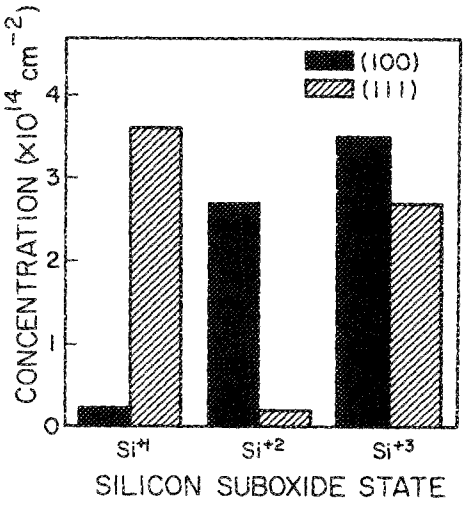

FIG. 8. Histogram summarizing the calculated areal densities of the Si^{+1}, Si^{+2}, and Si^{+3} suboxide states for (100)- and (111)-oriented substrates.

We observe a difference between Si(100) and Si(111) substrates in the width of the region over which the suboxide states are localized (again, excluding the Si^{+3} specie that extends beyond $0.3\langle\lambda_{oxide}\rangle$ into the near-interfacial SiO_2 network). For the (100) data of Fig. 5, the suboxide states are not removed until the oxide is less than $0.35\langle\lambda_{oxide}\rangle$ or ~10 Å. In contrast, the Si^{+1} intensity plotted in Fig. 7 for (111) does not appear to decrease until the oxide is less than $0.2\langle\lambda_{oxide}\rangle$ or ~6 Å. We cannot ascertain at the present time if this difference is real or if it represents a difference in the uniformity of the chemical etching between these two samples. It is also possible that the value of $\langle\lambda_{oxide}\rangle$ is different for (111) and (100). Based on the observed crystallographic dependence discussed below, however, we conclude that the suboxide species must be localized at the immediate SiO_2/Si interface and that the observed 6–10 Å width is due to broadening because of a small lateral nonuniformity in oxide thickness, compounded with the reaction depth of the chemical etchant.

B. Crystallographic dependence

If the suboxide species are indeed localized immediately at the SiO_2/Si interface, their distribution should depend upon the crystallographic orientation of the substrate. On an ideal unreconstructed Si(100) surface, each Si atom has two

TABLE I. Summary of suboxide concentrations at the SiO_2/Si interface (10^{14} cm^{-2}).

Substrate orientation	Oxidation conditions	Si^{+1}	Si^{+2}	Si^{+3}	Total no. of suboxides	Percentage of a monolayer
100[a]	900 °C, dry	0.2	2.7	3.5	6.4	94%
111[a]	900 °C, dry	3.6	0.2	2.7	6.5	83%
100[b]	900 °C, wet	0.1	3.0	2.7	5.8	85%
100[b]	900 °C, wet, POA	0.5	2.1	2.5	5.1	75%
100[b]	1000 °C, dry	0	3.2	2.7	5.9	87%
100[b]	1000 °C, dry, POA	0.5	2.3	2.6	5.4	79%

[a] This work.
[b] Reference 23, POA refers to 1150 °C post oxidation anneal in N_2 for 30 min.

unsatisfied bonds and should form only Si^{+2}. On a Si(111) surface, each Si atom has one unsatisfied bond and should form only Si^{+1} states. Such a preferential distribution is, indeed, observed in Fig. 8. The ideal interfaces are illustrated in the upper panel of Fig. 9. High-resolution transmission electron microscopy (TEM) studies have demonstrated, however, that the actual interface contains a number of monolayer steps.[1] As illustrated in the lower panel of Fig. 9, we suggest that step sites will give rise to suboxide distributions different from those ideally anticipated. Impurity sites, such as that illustrated with hydrogen in Fig. 9, will also produce core-level binding energy shifts for suboxide species other than those expected on an ideal interface. Thus, one might anticipate that all three suboxide species would be observed by photoemission on a given substrate orientation, but that the distribution would significantly favor Si^{+2} on (100) and Si^{+1} on (111). We suggest that the extent to which the experimental suboxide distribution deviates from the ideal is a measure of structural imperfections and/or impurities at the interface. Examination of the histogram in Fig. 8 clearly shows the strong crystallographic dependence suggested by the ideal interfaces illustrated in Fig. 9. For the Si(100) substrate, we observe at least a factor of 11 more Si^{+2} than Si^{+1} states (as discussed previously, the Si^{+1} value may be considered to be an upper limit). For the Si(111) substrate, precisely the opposite is observed—the amount of Si^{+1} observed exceeds the Si^{+2} by a factor of at least 17.

Interestingly, the amount of interfacial Si^{+3} observed is approximately the same for both substrate orientations. While there exists more error in the determination this component due to the difficulty in discriminating it from Si^{+3} states extending into the SiO_2 network, it is clear that this component is relatively large. We do not understand as yet why the Si^{+3} component is significantly larger than the Si^{+1} and Si^{+2} components on Si(100) and Si(111), respectively.

The simple model in Fig. 9 suggests that surface Si atoms not terminated in the Si^{+2} state on Si(100) or the Si^{+1} state on Si(111) reflect the presence of steps or impurity sites at the interface. From the data in Table I, we calculate that 40% and 46% of the interfacial substrate Si atoms for SiO_2 on Si(100) and Si(111), respectively, are ideally terminated as Si^{+2} and Si^{+1} states, respectively. This suggests that 60% to 54% of the substrate atoms at these interfaces are not ideally terminated because of steps and/or impurities. This estimation includes the contribution previously attributed to hydrogen termination of the substrate Si atoms [6% and 17% for these (100) and (111) samples, respectively]. These inferred values for step densities are significantly higher than the 3–27% interfacial step densities reported by Hahn and Henzler[28] for SiO_2 on Si(111) using spot-profile analysis of low-energy electron diffraction (LEED). Our values are also higher than those suggested in TEM studies by Krivanek *et al.*,[1] wherein it was observed that one-plane-high atomic step exist on the Si surface, separated by 20–40 Å, for SiO_2 on (100)-, (111)-, and (911)-oriented substrates. LEED and TEM are diffraction techniques, however, and require that an atomic step be extended in depth in order to be observed, i.e., a ledge rather than a few isolated steps. These techniques may therefore significantly underestimate the true step density. The suboxide distributions as measured here with XPS should be sensitive not only to ledges, but to point defects as well. Our results are supported by recent work by Goodnick *et al.*[29] which models the effect of projecting the two-dimensional interfacial roughness through a cross-sectional thickness to form the one-dimensional boundary layer observed in high-resolution TEM. They conclude that the actual interface is significantly rougher than indicated by the TEM micrograph.

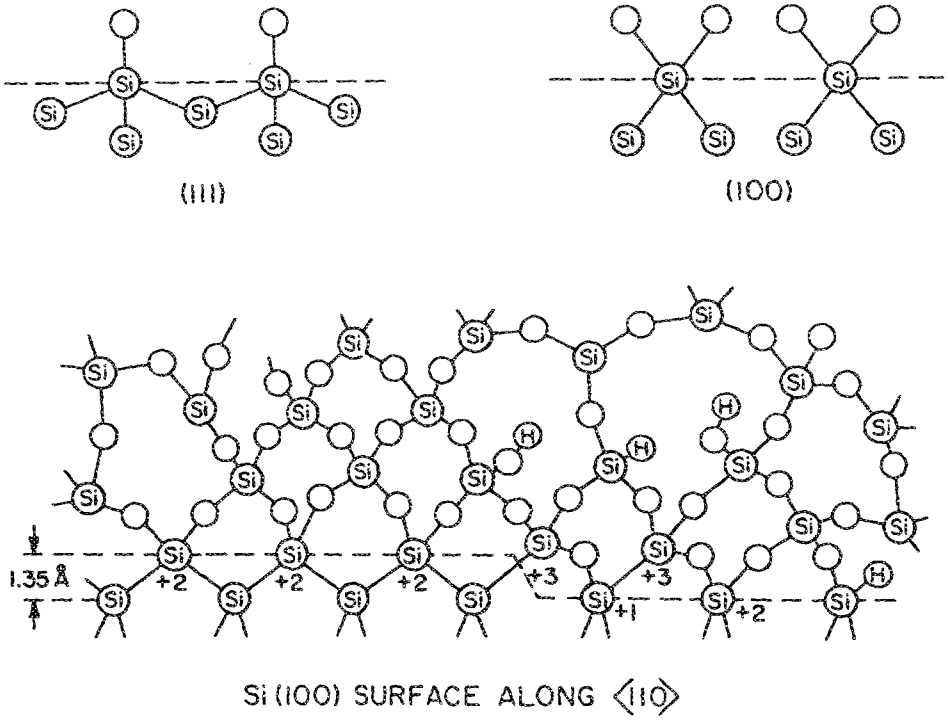

FIG. 9. Upper panel: suboxide states expected for ideal unreconstructed Si(100) and Si(111) interfaces. Lower panel: schematic illustration of how step and impurity sites give rise to suboxide states other than those ideally anticipated. The illustration is from a Si(100) interface.

The strong crystallographic dependence of the Si^{+1} and Si^{+2} intensities strengthens the suggestions in Sec. IV A that these species are located immediately at the abrupt transition between the SiO_2 and Si substrate. That their distribution so closely agrees with that expected for an ideal interface is an indication that the first few monolayers of substrate Si atoms are not significantly disordered relative to a bulk configuration. This is consistent with thin-crystal transmission channeling studies[4,20] which presented evidence only for strain at the Si substrate surface, but not for gross disordering.

The striking crystallographic dependence of the Si^{+1} and Si^{+2} suboxide states we observe appears to contradict the study by Hollinger and Himpsel[9] in which they reported the suboxide distribution to be independent of substrate orientation for thin oxides thermally grown *in situ* to 5, 7, and 11 Å in thickness.[8] Some orientation dependence is suggested, however, by their data for the thickest oxide sample. We can speculate that, if the substrates were cleaned by the conventional *in situ* approach of ion bombardment followed by a high-temperature thermal anneal, their starting substrates were most probably (7×7)Si(111) and (2×1)Si(100) reconstructions. It is likely that the distribution of suboxides produced when oxygen is exposed *in situ* to such reconstructed surfaces is quite different from that observed at interfaces of thicker oxides produced using typical device-quality processing conditions.

Our data agree well with the early photoemission studies of Raider and Flitsch.[7] They determined the average composition of an interfacial layer 25 Å in thickness by extrapolation of experimental Si 2*p* binding energies and intensities. They concluded an average interfacial composition of $SiO_{1.35}$ and $SiO_{1.13}$ for thermal oxides on (100) and (111) substrates, respectively. If we calculate average interfacial compositions by appropriately averaging the suboxide concentrations given in Table I, we obtain the values of $SiO_{1.33}$ and $SiO_{0.93}$ for Si(100) and Si(111) interfaces, respectively. These values compare quite favorably with the earlier work of Raider and Flitsch.

The work of Hattori and Suzuki[10] is also consistent with our results in that they also observe a predominance of Si^{+2} on Si(100) and Si^{+1} on Si(111). These authors disagree, however, in the localization of the Si^{+3} state and conclude that this suboxide is distributed throughout the bulk of the SiO_2, rather than being localized in the first ~30 Å of SiO_2 as reported here. Part of this difference may arise because of the assumptions made during the least-squares analysis of the suboxide intensities. Hattori and Suzuki assume that the line shape and position for SiO_2 at all oxide thicknesses are the same as those obtained for a 150 Å oxide. As explained in Sec. III, we take into account the observation that the Si 2*p* signal from the near-interfacial SiO_2 region is shifted in energy relative to bulk SiO_2. Because of the proximity of the signals for the Si^{+3} and near-interfacial SiO_2 (2.6 and 3.8 eV, respectively, relative to the substrate) omission of the latter from the analysis will result in increased intensity being assigned to the Si^{+3} state. This problem is exacerbated by the relatively low resolution obtainable from their unmonochromatized XPS spectrometer.

V. CONCLUSIONS

Using XPS in conjunction with chemical spin-etch profiling of thermal SiO_2 on (100)- and (111)-oriented substrates, we have examined the detailed composition of the SiO_x transition region at the SiO_2/Si interface. We find that Si^{+1} and Si^{+2} suboxide states are localized at the abrupt transition between SiO_2 and Si. The Si^{+3} state extends ~30 Å into the bulk SiO_2.

We observe a strong crystallographic dependence of the Si^{+1} and Si^{+2} suboxide states. The Si^{+1} state dominates at the SiO_2/Si(111) interface, while Si^{+2} dominates at the SiO_2/Si(100) interface, as anticipated from consideration of ideal unreconstructed (111) and (100) Si surfaces. We suggest that the existence of suboxide states other than Si^{+1} on Si(111) and Si^{+2} on Si(100) can be used to infer the presence of steps and impurity sites. This conclusion is consistent with the observed process dependence, to be reported elsewhere. We did not observe any crystallographic dependence for the Si^{+3} state.

For all cases examined, we find that less than one full monolayer of interfacial Si atoms can be attributed to bonding to oxygen as suboxides. The total number of Si^{+1}, Si^{+2}, and Si^{+3} suboxide states observed at the SiO_2/Si(100) interface corresponds to 6.4×10^{14} states/cm^2 (or 94% of a monolayers). For the (111) orientation, 6.5×10^{14} states/cm^2 (83% of a monolayers) were observed. We speculate that the remaining interfacial Si substrate atoms are terminated with hydrogen.

ACKNOWLEDGMENTS

The authors thank S.-T. Chang and M. D. Moyer for assistance with sample preparation. The work at the Xerox Corporation was supported by the U.S. Army Electronics Research and Development Command (ERADCOM). The work at the Jet Propulsion Laboratory, California Institute of Technology, was jointly supported by the National Aeronautics and Space Administration and the U. S. Department of Energy, Division of Solar Energy.

[1] O. L. Krivanek, D. C. Tsui, T. T. Sheng, and A. Kamgar, in *The Physics of SiO_2 and its Interfaces*, edited by S. T. Pantelides (Pergamon, New York, 1978), p. 356.
[2] T. E. Jackson, J. R. MacDonald, L. C. Feldman, P. J. Silverman, and I. Stensgaard, Surf. Sci. **100**, 35 (1980).
[3] N. W. Cheung, L. C. Feldman, P. J. Silverman, and I. Stensgaard, Appl. Phys. Lett. **35**, 859 (1979).
[4] R. Haight and L. C. Feldman, J. Appl. Phys. **53**, 4884 (1982).
[5] C. C. Chang, Proc. Electrochem. Soc., **78-3**, 106 (1978).
[6] C. R. Helms, Y. F. Strausser, and W. E. Spicer, Appl. Phys. Lett. **33**, 767 (1978).
[7] S. I. Raider and R. Flitsch, in *The Physics of SiO_2 and its Interfaces*, edited by S. T. Pantelides (Pergamon, New York, 1978), p. 384; J. Vac. Sci. Technol. **13**, 58 (1976); IBM J. Res. Dev. **22**, 294 (1978).
[8] F. J. Grunthaner, P. J. Grunthaner, R. P. Vasquez, B. F. Lewis, J. Maserjian, and A. Madhukar, J. Vac. Sci. Technol. **16**, 1443 (1979); Phys. Rev. Lett. **43**, 1683 (1979).
[9] G. Hollinger and F. J. Himpsel, Appl. Phys. Lett. **44**, 93 (1984).
[10] Takeo Hattori and Toshihisa Suzuki, Appl. Phys. Lett. **43**, 470 (1983).
[11] D. E. Aspnes and J. B. Theeten, J. Electrochem. Soc. **127**, 1359 (1980).
[12] F. J. Grunthaner and J. Maserjian, in *The Physics of SiO_2 and its Interfaces*, edited by S. T. Pantelides (Pergamon, New York, 1978), p. 389.
[13] J. M. Hill, D. G. Royce, C. S. Fadley, L. F. Wagner, and F. J. Grunthaner, Chem. Phys. Lett. **44**, 225 (1976).

[14]P. J. Grunthaner, Jet Propulsion Laboratory publication No. 85-77 (1985); See also Ref. 8.
[15]M. H. Hecht, F. J. Grunthaner, P. Pianetta, L. I. Johansson, and I. Lindau, J. Vac. Sci. Technol. A2, 584 (1984).
[16]M. H. Hecht and F. J. Grunthaner, in *Spectroscopic Characterization Techniques for Semiconductor Technology II* (Society of Photo-Optical Instrumentation Engineers, Bellingham, Washington, 1985), Vol. 524, p. 18.
[17]J. Finster, D. Schulze, F. Bechnstedt, and A. Meisel, Surf. Sci. **152/153**, 1063 (1985).
[18]R. Williams and A. M. Goodman, Appl. Phys. Lett. **25**, 531 (1974).
[19]R. L. Mozzi and B. E. Warren, J. Appl. Crystallogr. **2**, 164 (1969).
[20]L. C. Feldman, P. J. Silverman, J. S. Williams, T. E. Jackson, and I. Stensgaard, Phys. Rev. Lett. **41**, 20 (1978).
[21]R. P. Vasquez and F. J. Grunthaner, Surf. Sci. **99**, 681 (1980).
[22]J. M. Hill, M. S. thesis, University of Hawaii, Honolulu (1975).
[23]M. H. Hecht, P. J. Grunthaner, and F. J. Grunthaner, in *Proceedings of the 17th International Conference on the Physics of Semiconductors*, edited by J. D. Chadi and W. A. Harrison (Springer, New York, 1985), p. 219.
[24]An error was made in the calculation of the oxide thickness reported in Ref. 23. The x-axis maximum in Fig. 3 of Ref. 23 should read ~ 30 Å rather than 20 Å. The incorrect figure is reproduced in F. J. Grunthaner, P. J. Grunthaner, M. H. Hecht, and D. Lawson, in *Insulating Films on Semiconductors*, edited by J. J. Simone and J. Buxo (Elsevier, New York, 1986), p. 1.
[25]K. H. Beckman and N. J. Harrick, J. Electrochem. Soc. **118**, 614 (1971).
[26]R. Gale, F. J. Feigl, C. W. Magee, and D. R. Young, J. Appl. Phys. **54**, 6938 (1983).
[27]S. M. Sze, *Physics of Semiconductor Devices* (Wiley, New York, 1981), p. 38.
[28]P. O. Hahn and M. Henzler, J. Vac. Sci. Technol. A2, 574 (1984).
[29]S. M. Goodnick, D. K. Ferry, C. W. Wilmsen, Z. Lilental, D. Fathy, and O. L. Krivanek, Phys. Rev. B **32**, 8171 (1985).